Chapter 2. Overview of X-ray Detection Technologies

2.1 X-ray Generation and Spectra

X-rays are an electromagnetic radiation having wavelengths that lie within a range of $\lambda = 0.001$ to 10 nm (nanometer), i.e. photon energies E = 120 eV to 1.2 MeV [CHE96]. Higher energy (shorter wavelength) photons are called γ-rays, and lower energy radiation (longer wavelength) photons are called ultraviolet (UV). These definitions can be found in [CLA27] [LIV66] [KAE67] [LIT79] [HAK96].

2.1.1 X-ray generation

It was Roentgen who first announced discovery of this radiation in 1895 during the course of some experiments with cathode rays, which are streams of electrons in vacuum tubes. In Roentgen's investigations of the properties of x-rays he found that x-rays are generated whenever cathode rays strike a solid body and are stopped by it. Thus, in order to generate x-rays, three main components are required, namely, a source of charged particles, a means of accelerating them and a solid target to stop them [BRO66]. Electrons are generally used as the charged particles and are accelerated by a voltage ranging from a few hundreds volts to hundreds of kilovolts. When accelerated electrons hit a target, the kinetic energy of those electrons is converted to heat and x-rays.

The x-ray tube is one type of generator and is used widely in x-ray scanning systems. X-ray tubes mainly consist of a solid metallic target used as an anode, a filament used as a cathode, and two circuits to heat the filament and drive electrons to the anode. An x-ray source is schematically shown in Figure 2.1-1. Tungsten is commonly used as a target material, because of its good heat conductivity and high melting point [MIC93].

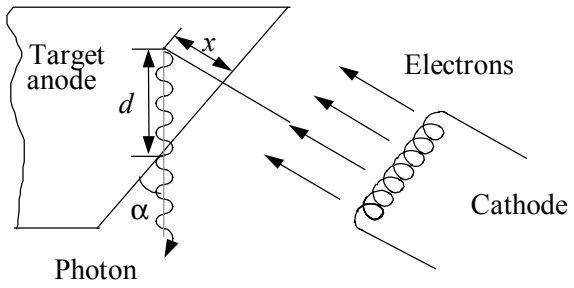

Figure 2.1-1 Schematic description of x-ray tube. Here α is the target angle, d is the x-ray photon path length through the target, and x is the depth of electron penetration into the target material.

2.1.2 The characteristic spectra

Some electrons from the cathode, when hitting the target (known as anode in Figure 2-1), may have enough energy to produce ions by removing inner electrons from the atom, even down to the innermost or K-shell. Such an ion has a low-energy hole in its electronic structure, and this vacancy is promptly filled when one of its electrons in a higher energy state falls to this low-energy level. When an electron falls into a low-energy level, energy is released in the form of x-rays having particular wavelengths which are characteristic of the

target material. Therefore, x-rays generated by this mechanism are called characteristic x-rays.

Characteristic emission lines can only result from transitions of electrons of atoms in the target material between allowed orbits (Figure 2.1-2), as predicted by quantum theory which states that every electron in a given atom moves on an orbital that is characterized by four numbers [GRI93]:

- n, the principal quantum number, or Bohr number, is associated with successive orbitals. n takes a positive integer 1, 2, 3, 4, … , that designates the K, L, M, N, … shells respectively.
- l, the angular quantum number, is a measure of the orbital angular momentum which accounts for the existence of elliptic and circular electron orbitals. It can take all integer values between 0 and (n-1), inclusive. $l = 0$ corresponds to a circular orbit.
- s, the spin quantum number, can only take two possible values: +1/2 and –1/2. It is often represented by + and -.
- j, the total angular quantum number. Its value is calculated as $l \pm s$, and must be greater than 0. Each possible value of j for a particular orbital determines a unique energy level.

The selection rules that govern "allowed" transitions between states are [BRO66],

$$\left.\begin{array}{l} \Delta n \text{ is arbitrary} \\ \Delta l = \pm 1 \\ \Delta j = \pm 1, 0 \end{array}\right\} \qquad (2.1)$$

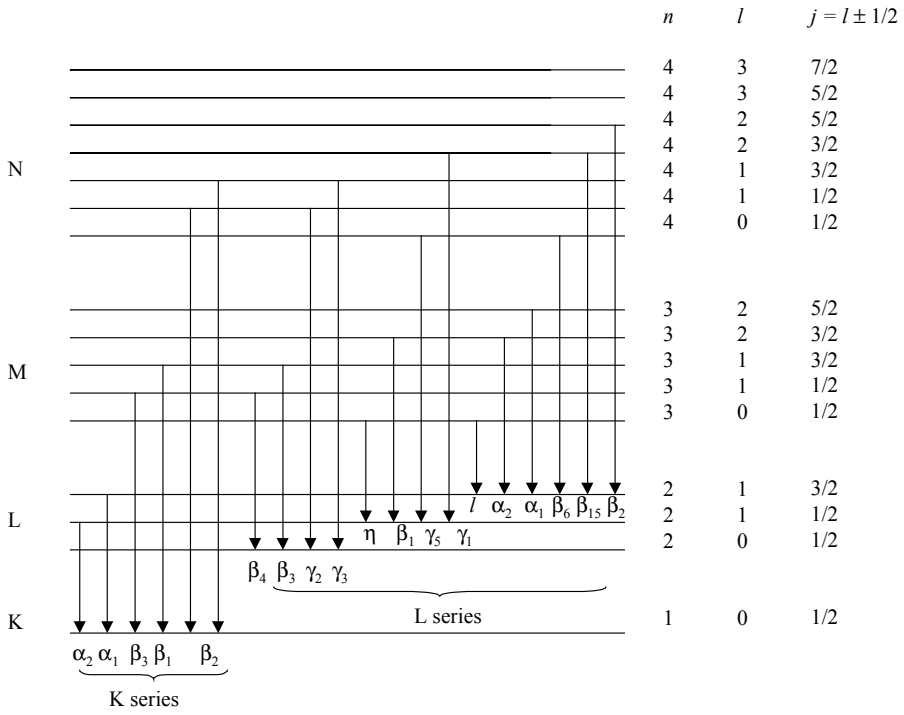

Figure 2.1-2 Energy levels and characteristic x-ray transitions. Each energy level can be determined by the principal quantum number n, the angular quantum number l, and total angular quantum number j. The diagrams contain all the lines of K series and L series for the transitions between K, L, M, and N [DYS93].

where $\Delta l = \pm 1$ corresponds to the emission of the dipole radiation, and is the most likely class of transition. Transitions for which $\Delta l = \pm 2$ are occasionally observed, though with reduced intensity. These are known as electric quadrupole transitions.

By using the above selection rules, the properties of characteristic spectra can be determined. The further discussions on this issue can be found in the following resources. An analytical expression for the location of the lines is given in [GRI93], a review with a full list of references for the width of lines can be found in [BAM72], and the experimental determination and analysis for the relative line intensities are given in [RAO72].

2.1.3 The continuous spectra of x-rays

According to classical electromagnetic theory, there is no lower limit to the wavelength of the radiation that a moving electron can produce when it is stopped suddenly. But there is a quantum limit. Given an electron has been accelerated through a difference of potential of V_0 volts, we can use Equation (2.2), known as the Duane-Hunt law, to compute the wavelength of the resulting radiation if the electron loses all its energy in a single encounter,

$$\lambda_{\min} = \frac{hc}{eV_0} \tag{2.2}$$

where h is Planck's constant, c is the velocity of light, and e is the electron charge. In this case the energy loss of the electron in eV is numerically equal to the accelerating potential in volts. Therefore we have,

$$\lambda_{\min} = \frac{6.63\times10^{-34}[\mathrm{J}\cdot\mathrm{sec}]\cdot 3.00\times10^{8}[\mathrm{m}\cdot\mathrm{sec}^{-1}]}{1.60\times10^{-19}[\mathrm{C}]\cdot V_0[\mathrm{V}]} = \frac{1240}{V_0}[\mathrm{nm}] \tag{2.3}$$

This expression gives the minimum wavelength, since no electron can lose more energy than it has, and there will be a continuous distribution of radiation toward longer wavelengths because there are all sorts of collisions, from direct hits to glancing ones. Thus glancing collisions account for the continuous spectrum of x-rays from any target material and also for the inefficiency of the conversion of electron energy into x-ray energy. The Germans named this continuous radiation "bremsstrahlung", meaning literally “braking radiation.” This is a highly descriptive term, since it refers to the radiation that results from the braking or stopping of charged particles [ENG72].

The shape of the bremsstrahlung spectrum depends primarily on the kinetic energy of the incident electrons, with a small dependence in the nature of the target. The earliest well-known theoretical model of the bremsstrahlung spectra for thick targets was developed in 1923 [KRA23],

$$E\,N(E)dE = K\,Z(T - E)dE \tag{2.4}$$

where E is the energy of x-ray photons produced, $N(E)dE$ is the number of x-ray photons produced with an energy between E and $E+dE$ per incident electron, K is a constant, Z is the target atomic number, and T is the electron’s kinetic energy. The model is widely applied, because of its simplicity and general agreement with the experimental results. However, it does not consider the electron energy distribution and ignores the attenuation of photons in the target itself. More recently, several semi-experimental models for generating x-ray spectra have been developed. Soole developed a model to simulate x-ray spectra that took into account energy reduction of electron within the target material [SOO72]. Birch and Marshall extended and modified the work of Soole and published results that were in good agreements with the measured spectra [BIR79].

XL [XIE95], an *X*-ray imaging simulator for *L*uggage inspection developed at Virginia Tech, has developed its own x-ray source model for the continuous tungsten spectrum based on the semi-experimental models of Soole and Birch and Marshall. A comparison of the computed spectrum from XL with the spectrum measured by [FEW81], at incident electron energies of 70 keV and 140 keV, with and without considering the line spectra respectively, are shown in Figure 2.1-3 and Figure 2.1-4. The relative errors at incident electron energies are about 10% and 5% without and with line spectra, respectively [ABB96].

The XL source model can be written as follows,

$$
\begin{aligned}
N(E)dE = {} & \frac{N_A \rho}{A} \int_E^{T_0} \left(1 + \frac{T}{m_0 c^2}\right) \\
& \times \frac{Z^2}{T} \left(0.503 - 0.94597\left(\frac{E}{T}\right) + 0.1553\left(\frac{E}{T}\right)^2 + 1.1632\left(\frac{E}{T}\right)^3 - 0.6818\left(\frac{E}{T}\right)^4\right) \frac{dE}{E} \\
& \times \left(\frac{1}{A_{msp} + B_{msp} e^{-TC_{msp}}}\right) \\
& \times \left\{\exp\left[-\left(a_1 + a_2\left(\frac{E}{100}\right)^{-1.6} + a_3\left(\frac{E}{100}\right)^{-2.7} + a_4\left(\frac{E}{100}\right)^{-3.5} + a_5\left(\frac{E}{100}\right)^{-4.5}\right)\left(\frac{T_0^2 - T^2}{\rho C \sin\alpha}\right)\right]\right\} dT \\
& + K_\alpha + K_\beta
\end{aligned}
\tag{2.5}
$$

The parameters are defined as:

$T =$	Electron's kinetic energy
$T_0 =$	Initial kinetic energy that is assumed to impinge on the target material

Z = Target atomic number

A = Target atomic mass

ρ = Target density

E = X-ray photon's energy

N_A = Avogadro's number

A_{msp}, B_{msp}, C_{msp} = Three parameters related to the mass stopping power dT/dx, and have been estimated (see Table 2.1-1) using least-squares techniques by [TUC91]

C = Thomson-Whiddington constant (see Table 2.1-2) that is related to the selected incident energies [BIR79]

a_1, a_2, a_3, a_4, a_5 = Mass attenuated coefficients (see Table 2.1-3) estimated by [BEV69], and refined by [TUC91]

dE, dT = Energy step sizes

$m_0 c^2$ = Rest mass energy of the electron

K_α, K_β = Characteristic spectra for tungsten target, are estimated by combining experimental data [FEW81] with relative intensity calculations [CHE96]

Table 2.1-1 Mass stopping power parameters for tungsten [TUC91].

A_{msp}	B_{msp}	C_{msp}
202.41 $keVm^2kg^{-1}$	1036.1 $keVm^2kg^{-1}$	0.04695 keV^{-1}

Table 2.1-2 Thomson-Whiddington constants for different incident electron energies [BIR79].

Electron Energy (T) (keV)	T-W constant (C) (keV^2m^2/kg)
50	0.54×10^5
75	0.625×10^5
100	0.7×10^5
150	0.84×10^5
200	1.0×10^5

Table 2.1-3 Parametrization of the mass attenuation coefficients of tungsten from 20 keV to 200 keV, $u=E/$(100 keV) [TUC91].

$\mu(u)/\rho = a_1 + a_2u^{-1.6} + a_3u^{-2.7} + a_4u^{-3.5} + a_5u^{-4.5}$					
Energy	a_1 (m^2/kg)	a_2 (m^2/kg)	a_3 (m^2/kg)	a_4 (m^2/kg)	a_5 (m^2/kg)
E<69.5 keV	2.394×10^{-2}	-1.401×10^{-2}	1.023×10^{-1}	-4.795×10^{-3}	1.318×10^{-1}
E≥69.5 keV	4.312×10^{-2}	-3.636×10^{-1}	1.486×10^{0}	-9.404×10^{-1}	2.184×10^{-1}

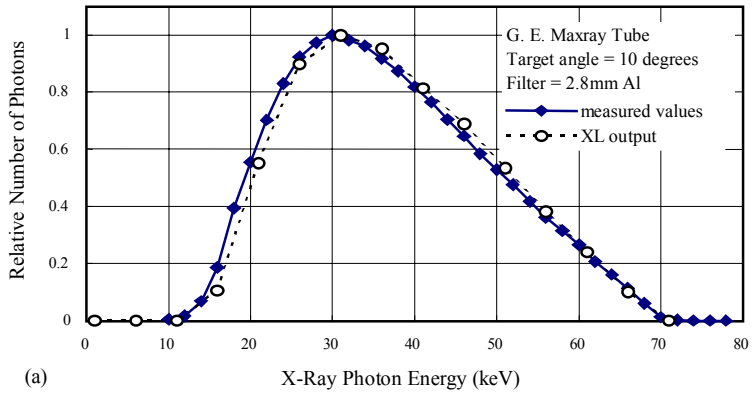

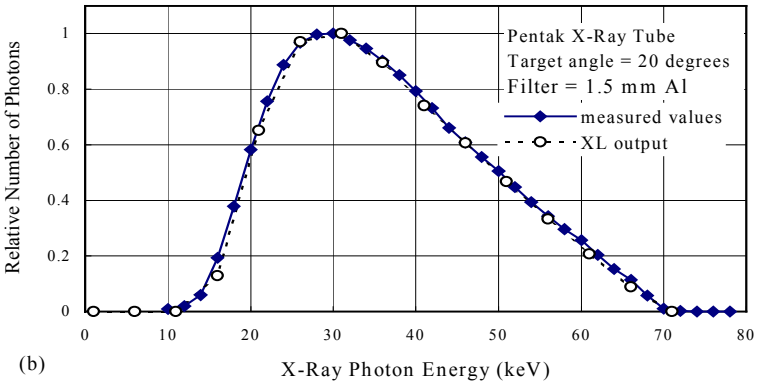

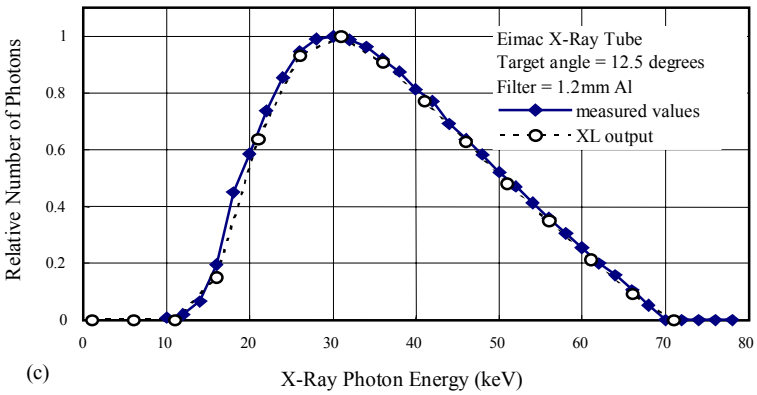

Figure 2.1-3 Spectra simulated by XL and measured by [FEW81], for an incident electron energy of 70 keV: (a) for a GE Maxray tube, (b) for a Pentak x-ray tube, and (c) for an Eimac x-ray tube [XIE95].

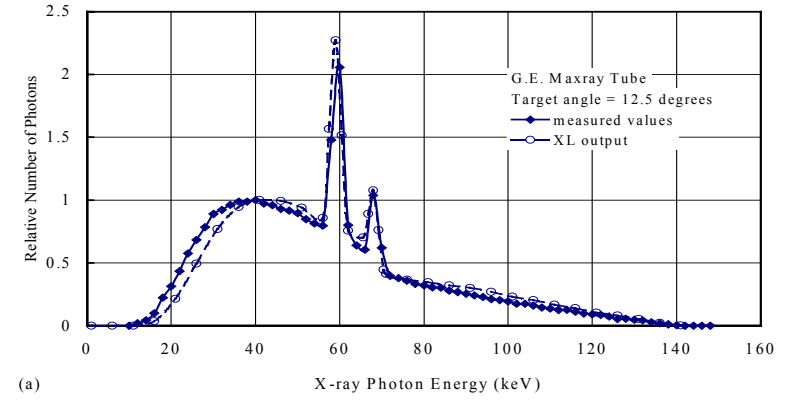

(a)

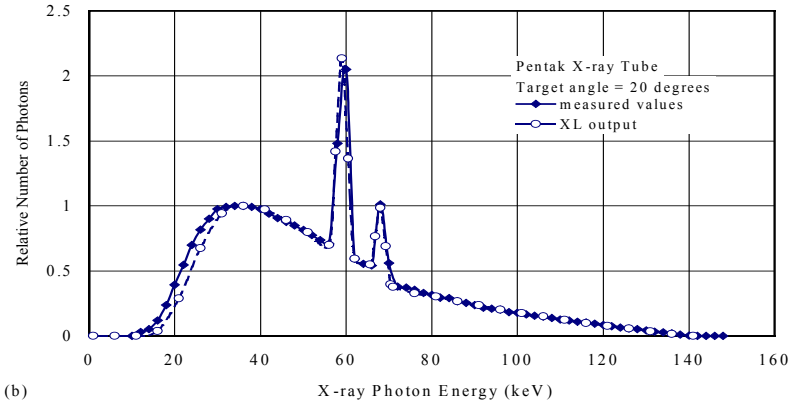

(b)

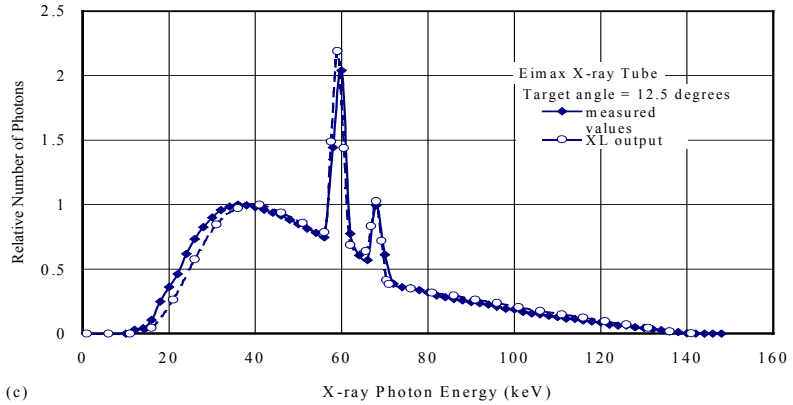

(c)

Figure 2.1-4 Comparison of simulated spectrum with the spectrum measured by [FEW81] for incident electron energy of 140 keV: (a) for a GE Maxray tube, (b) for a Pentak x-ray tube, and (c) for an Eimac x-ray tube [CHE96].

2.2 The Absorption and Scattering of X-rays

2.2.1 Introduction

A variety of physical processes are involved in the interaction of x-rays with matter [ATT68][SEL94]. On passing through matter, an x-ray beam undergoes attenuation; that is, its intensity decreases gradually by absorption and scattering. Absorption refers to the case in which an incident x-ray photon gives up all of its energy. Scattering refers to those x-ray photons that have undergone a change in direction after interaction with atoms of matter. Other photons are neither absorbed nor scattered; they simply pass through matter. This process is known as transmission.

When an x-ray beam interacts with matter, four major processes of attenuation exist: (1) the photoelectric effect, (2) coherent scattering, (3) incoherent (or Compton) scattering, and (4) pair production. The photoelectric effect corresponds to absorption and is one of the predominant interactions in the energy range of 1-100 keV. Coherent scattering and incoherent scattering contribute to a beam's attenuation by scattering the incident photons with and without energy change, respectively. Coherent scattering makes a major contribution at low photon energies (less than 50 keV) for high Z materials, where Z is the atomic number of a substance. Incoherent scattering is almost independent of photon energy. Pair production can only occur at energy levels greater than $2mc^2$, which is about 1.022 MeV [BRO66]. The essential feature is the disappearance of the photons and its replacement by a positron-electron pair [DYS90]. Pair production is not considered here since the energy range of x-rays commonly used for explosives detection is from approximately 10 keV to 150 keV.

2.2.2 The photoelectric effect

The photoelectric effect is the process by which an incident photon of energy *E* interacts with an orbital electron and ejects several fluorescent photons and an orbital electron. The electron must have binding energy *e* that is less than the energy of the incident photon. The incident photon is absorbed by the atom and loses all its energy. The atom responds by ejecting an electron, usually from the K or L shell, leaving a hole in that shell (see Figure 2.2-1) [SEL94]. Now the atom is ionized and is in an excited state. Generally, the inner electrons are the predominant contributors to the photoelectric effect. The energy of the incident photon ultimately results in freeing the electron from its shell and setting it in motion as a "photoelectron". For low energy x-rays, the photoelectric effect is the dominant process.

The photoelectric effect is characterized by the photoelectric absorption coefficient, also known as the "photoelectric cross section σ_{pe}". It represents the effective cross sectional area of an atom, and is related to the probability that an interaction will take place between an x-ray photon and an atom. The photoelectric cross section σ_{pe} in barn/atom (10^{-24} cm^2/atom) can be approximated, in the x-ray energy range of several keV to hundreds of keV, by the relationship:

$$\sigma_{pe} \approx 10\frac{Z^{4.5}}{E^3} \tag{2.6}$$

where *Z* is the atomic number of the target atom and *E* is the photon energy in keV [HUB69].

The relationship indicates that σ_{pe} increases as the atomic number *Z* (or the effective atomic number Z_{eff} for a compound) increases. On the other hand, it decreases as the x-ray photon

energy increases. This is a major factor that was used to distinguish organic (low-Z) materials from inorganic (high-Z) materials by early x-ray machines.

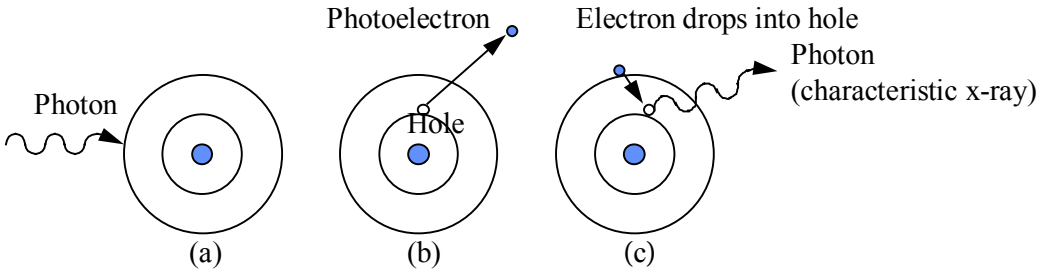

Figure 2.2-1 Photoelectric effects of interaction and absorption. (a) An incident photon loses all its energy on entering an atom, being absorbed in the process. (b) The atom responds by ejecting an inner shell electron, which becomes a photoelectron. The atom is now in an excited state. (c) An electron from a higher energy level fills the vacancy in the K-shell or L-shell, and emits a characteristic x-ray photon.

2.2.3 Coherent scattering

Coherent scattering (sometimes referred to as Thomson and Rayleigh scattering) occurs from strongly bound electrons, if a very low energy x-ray photon interacts with a strongly bound electron that may be set into vibration. It involves no energy loss, but results in the deflection of the incident x-ray photon from its original path, as shown in Figure 2.2-2 [SEL94]. The energy of photons determines the wavelength, following the relation $E=hc/\lambda$, where λ is the wavelength, c is the velocity of light, and h is Planck's constant. The incident photon has been scattered without undergoing any change in wavelength, frequency, or energy.

Convenient analytical expressions for the cross-section of coherent scattering do not seem to exist. But for the x-ray wavelengths less than the diameter of the scattering atoms, it is given as [DYS90],

$$\sigma_{coh} = 8\pi r_e^2 Z^2 \left(\frac{\lambda}{4\pi a_{TF} Z^{-\frac{1}{3}}} \right)^2 \left(0.8 - \frac{\lambda}{8 a_{TF} Z^{-\frac{1}{3}}} \right) \tag{2.7}$$

where $a_{TF} = 0.885$, and r_e is the classical electron radius. This leads to an approximately the following dependence, and is restricted, at least in the case of heavier elements, to x-ray energies greater than 60 keV [DYS90],

$$\sigma_{coh} \propto Z^{\frac{8}{3}} E^{-2} \tag{2.8}$$

At low photon energies (less than 50 keV), coherent scattering represents the major contribution to x-ray scattering. As the energy of the incident photon increases, the coherent scattering becomes small and can be ignored.

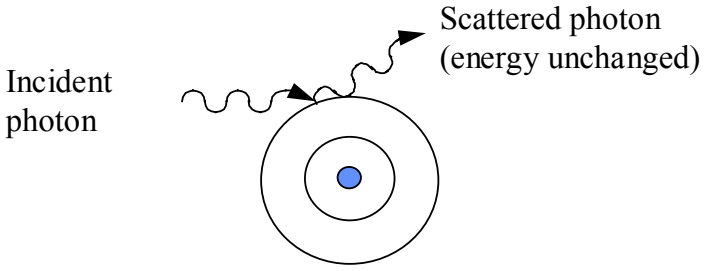

Figure 2.2-2 Schematic description of coherent scattering. The entering photon has undergone a change of direction only.

2.2.4 Incoherent (Compton) scattering

Incoherent (Compton) scattering is a process in which a photon interacts with a loosely bound electron that may be considered free and dislodged, and then the photon proceeds in a different direction, as shown in Figure 2.2-3 [SEL94]. The dislodged electron is called a Compton electron. Incoherent scattering involves both energy loss and the deflection of an x-ray photon path. Therefore, Compton scattering acquires a certain amount of kinetic energy that must be subtracted from the energy of the incident photon, in accordance with the law of conservation of energy. The wavelengths, frequency, or energy of scattered and incident x-rays are different. A scattered photon, in turn, performs in the same way as the incident photon interacts with matter.

At the energy range commonly used in explosives detection systems, scattering is dominated by the incoherent component. Incoherent scattering is not considerably affected by changes in the x-ray photon energy, and is roughly given by [HUS92]

$$\sigma_{ncs} = 0.665\, Z \text{ [barn/atom]} \tag{2.9}$$

For organic materials (low Z) and higher photon energy, x-ray attenuation is primarily governed by Compton scattering, due to the photoelectric effect decreases faster and is relatively small.

2.2.5 Characterization of x-ray attenuation processes

At the energies commonly used in luggage inspection systems, x-rays are either absorbed or scattered by objects in the luggage. The total x-ray cross section is a function of x-ray photon

energy and atomic number of matter. From previous descriptions, some discussions are given below:

- The photoelectric cross section σ_{pe} is strongly dependent on both energy and Z. For high-Z materials at a low energy range, σ_{pe} decreases more rapidly, and is much higher than for low-Z materials. This is a major factor that was used to distinguish organic (low-Z) materials from inorganic (high-Z) materials by early x-ray machines.
- The total effect of the three cross sections is that σ decreases as the energy of a photon increases. When x-rays pass through any particular material, the attenuation at energy E_1 over the attenuation at higher energy E_2 will give information about that material. Dual-energy systems utilize this property to classify materials, though there exists ambiguity due to the polychromatic spectrum in practical systems.
- The photoelectric effect dominates at low photon energies for both high Z and low Z materials, which will overpower the contribution of the coherent scattering. As the energy of the incident photon increases, the Compton effect first becomes the predominant type of interaction for low Z materials (at about 20 keV)., and then for high Z materials (at about 100 keV).
- The cross sections for Compton scattering do not vary much as a function of the photon energy, and can provide information about light materials. The principal reason is that the Compton signals from heavier materials are suppressed by photoelectric attenuation, allowing the light materials to stand out clearly.
- Coherent scattering, therefore, is not treated individually in this dissertation due to two reasons: (1) it is not the major process of absorption in x-ray scanning energies; (2) it may not be discriminated from Compton scattering by the detector in real x-ray luggage scanning systems.

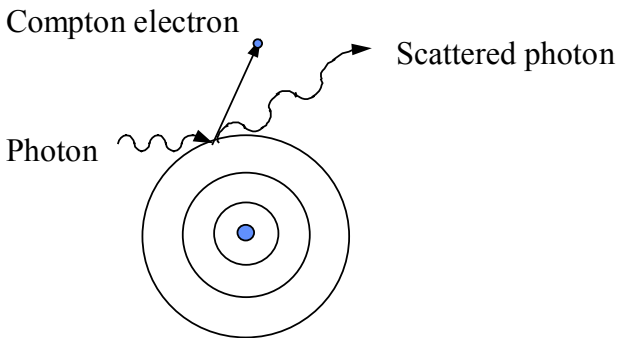

Figure 2.2-3 Compton interaction and scattering. Part of the photon's energy has been used up in removing a loosely bound orbital electron. Therefore, the emerging photon has less energy, and it has also undergone a change in direction.

2.3 X-ray Detectors

There are many types of detectors suitable for use with x-rays, such as x-ray film, channel electron multipliers, gas detectors, silicon detectors, and scintillation detectors. All the methods use some physical effect of x-ray on matter, e.g., the production of heat, the reduction of the electrical resistance, the emission of light, the production of gaseous ions and the photographic effect. We will focus on scintillation detectors, which are energy dispersive and are commonly used in x-ray scanning systems.

In this section, structure of scintillation detectors and processes involved in x-ray detection and measurement are presented. A mathematical expression of the detected signal for a particular x-ray imaging system will be addressed in Chapter 3.

2.3.1 Structure of scintillation detectors

The operation of a scintillation detector depends on the luminescence of a crystal when excited by ionizing radiation. Photons are produced in the visible region and then are allowed to impinge on a photodiode. The photodiode converts the energy of visible photons to an electrical current, which is then sensed electronically. Scintillators are usually classified as organic or inorganic. Inorganic scintillators are preferred for x-ray studies because of their high level of photoelectric absorption.

The structure of a scintillation detector is shown in Figure 2.3-1 [TAK90]. X-rays enter a scintillator material, and produce visible photons by luminescence. These visible photons pass through a film and are detected by a photodiode. The mirror-polish scintillator is normally surrounded with an optical light reflector to ensure maximum channeling of light to the photodiode. One face of the scintillator is covered with a transparent film that is in contact with the photodiode, in order to smooth remaining craters on the polished surface to ensure maximum transmission of light.

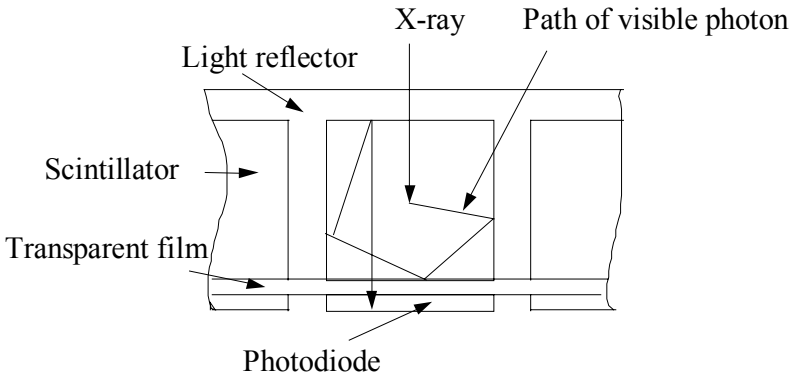

Figure 2.3-1 Schematic illustration of the structure of an x-ray detector. An x-ray photon is converted to visible photons, which are detected by a photodiode after several reflections on surfaces of the scintillator.

2.3.2 Processes involved in x-ray detection and measurement

An x-ray photon impinges on the scintillator where it dissipates its energy in the ionization and excitation of the molecules. A fraction of this energy is converted into light photons that are radiated in all directions. These light photons have a main emission wavelength region. Finally, the emitted light photons fall on the photodiode through the transparent film directly or after reflection from the surfaces of the scintillator in contact with the light reflectors.

The operation of the scintillation detector can be divided into four distinct, consecutive stages:

- The absorption of the incident radiation by the scintillator.
- The luminescent conversion of the energy dissipated in the scintillator, and the emission of light photons.
- The collection of the emitted light photons to the photodiode.
- The absorption of light photons at the photodiode.

The electrical output of the photodiode can be measured or even amplified to indicate the intensity of the incident x-ray photons.

2.4 Principles of X-ray Detection

X-ray detection methods are most widely used to inspect luggage at the airport. This section presents some results in x-ray physics, which is fundamental of x-ray imaging systems.

When a beam of x-rays of energy E and initial intensity I_0 traverses through a material of thickness t, its intensity I is reduced exponentially [MCM92],

$$I = I_0 e^{-n\sigma t} \tag{2.10}$$

where t is commonly given in cm, I and I_0 are given in keV, and σ is the total cross section in cm^2/atom. The quantity σ is the sum of two independent cross sections in the energy range typically used to screen airport luggage: photoelectric cross section σ_{pe}, and photon scatter cross section σ_{sc}. Both σ_{pe} and σ_{sc} are the function of atomic number and x-ray energy, as they have been discussed in Section 2.2:

$$\sigma(Z,E) = \sigma_{pe}(Z^{4.5}, E^{-3}) + Z \cdot \sigma_{sc}(E) \tag{2.11}$$

For a given elemental substance, the number of atoms per unit volume, n, is calculated from,

$$n = \frac{N_A \rho}{A} \tag{2.12}$$

where N_A (6.02252×10^{23} atom/mole) is Avogadro's number, A is the atomic weight in g/mole, ρ is the density of the substance in g/cm^3, and n is in atoms/cm^3.

The total cross section per atom σ, when multiplied by the number of atoms per unit volume of matter, is the linear attenuation coefficient μ, which is per centimeter of travel in the matter. The function used to calculate the linear attenuation coefficient μ is as follows:

$$\mu\,[\mathrm{cm^{-1}}] = \sigma\left[\frac{\mathrm{cm^2}}{\mathrm{atom}}\right] \cdot \rho\left[\frac{\mathrm{g}}{\mathrm{cm^3}}\right] \cdot \frac{N_A}{A}\left[\frac{\mathrm{atom}}{\mathrm{g}}\right] \tag{2.13}$$

If the linear attenuation coefficient, μ, is used, the attenuation of photons in homogeneous matter can be defined by the exponential law:

$$I = I_0 e^{-\mu t} \tag{2.14}$$

Taking the logarithm of both sides and writing it explicitly, we obtain,

$$\ln(I_0 / I) = \mu t = \sigma(Z, E)\frac{N_A}{A}\rho t \tag{2.15}$$

It is known from Equation (2.15) that x-ray attenuation through an object is a function of the material composition, density, thickness, and x-ray spectral distribution. There are a number of methods in which the fundamental interactions outlined above can be used to identify materials.

2.5 X-ray Imaging systems

2.5.1 Conventional x-ray screening systems

Conventional x-ray screening systems measure the attenuated x-ray energy after it has passed through a scanned object. They were introduced to combat hijacking in 1970's. The devices were designed to give high-resolution pictures with a good dynamic range of gray scale so that the security operator could identify weapons, such as guns and knives, made of metals in characteristic shapes.

Some early x-ray machines being offered as explosives detection systems (EDS) were, for the most part, adaptations of the existing technologies above to the EDS problems, so that

these devices might make evident explosives made from light materials with no characteristic shape. Two image examples are given in Figure 2.5-1 and Figure 2.5-2.

Consider the x-ray signal obtained in a projected image of an explosive shown in Figure 2.5-3. The integrated signal, S_{bomb}, is simply [GRO91],

$$S_{bomb} = Na_i \log(I_0 / I) = \sigma(Z,E)\frac{N_0}{A}\rho t N a_i = \sigma(Z,E)\frac{N_0}{A}M \tag{2.16}$$

where N is the number of pixels covering the bomb's projected area, a_i is the area of each pixel and M is the mass of the bomb. The sum of the logs of attenuation ratios, due only to the bomb, is proportional to the mass of the bomb. It is assumed, for simplicity, a constant thickness of penetration but the answer is in general, independent of the shape.

The total signal from a bag, S_{bag}, is the sum of the signals from every component in the bag. Thus, a small explosive in a large, heave suitcase filled with a lot of materials will yield a bomb signal S_{bomb} that only takes a few percent of the S_{bag}. If heavier materials, such as iron S_{iron}, are present then the ratio for that object will be greater. Suppose that we set our threshold equal to S_{bomb}, we will false alarm on almost every heavy inspected object. The total attenuation is therefore not enough to find small bombs, though it will be an important input in more general EDS schemes.

2.5.2 Dual-energy x-ray imaging systems

Some commercial x-ray imaging systems at airports now feature dual-energy analysis to estimate the atomic numbers of the materials in luggage bags, a vital piece of information for the security operator [KRU91] [ELB92]. To see the power and limitations of the method,

consider again the simple object in Figure 2.5-3. The logarithm attenuation signal obtained at x-ray energy E_1 is given in Equation (2.15) [GRO91],

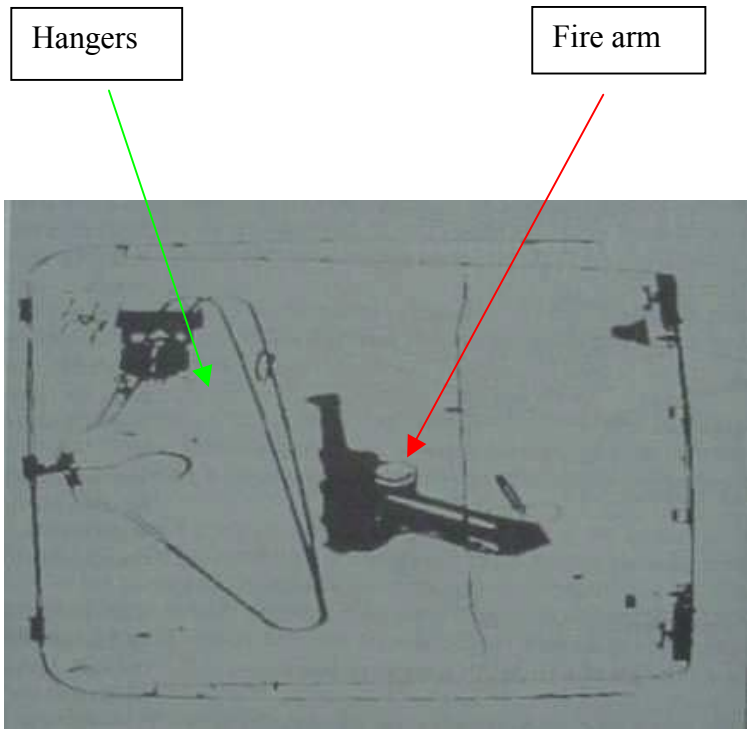

Figure 2.5-1 An image example to show regions of high attenuation. The raw object shapes represent possible threats [BER92].

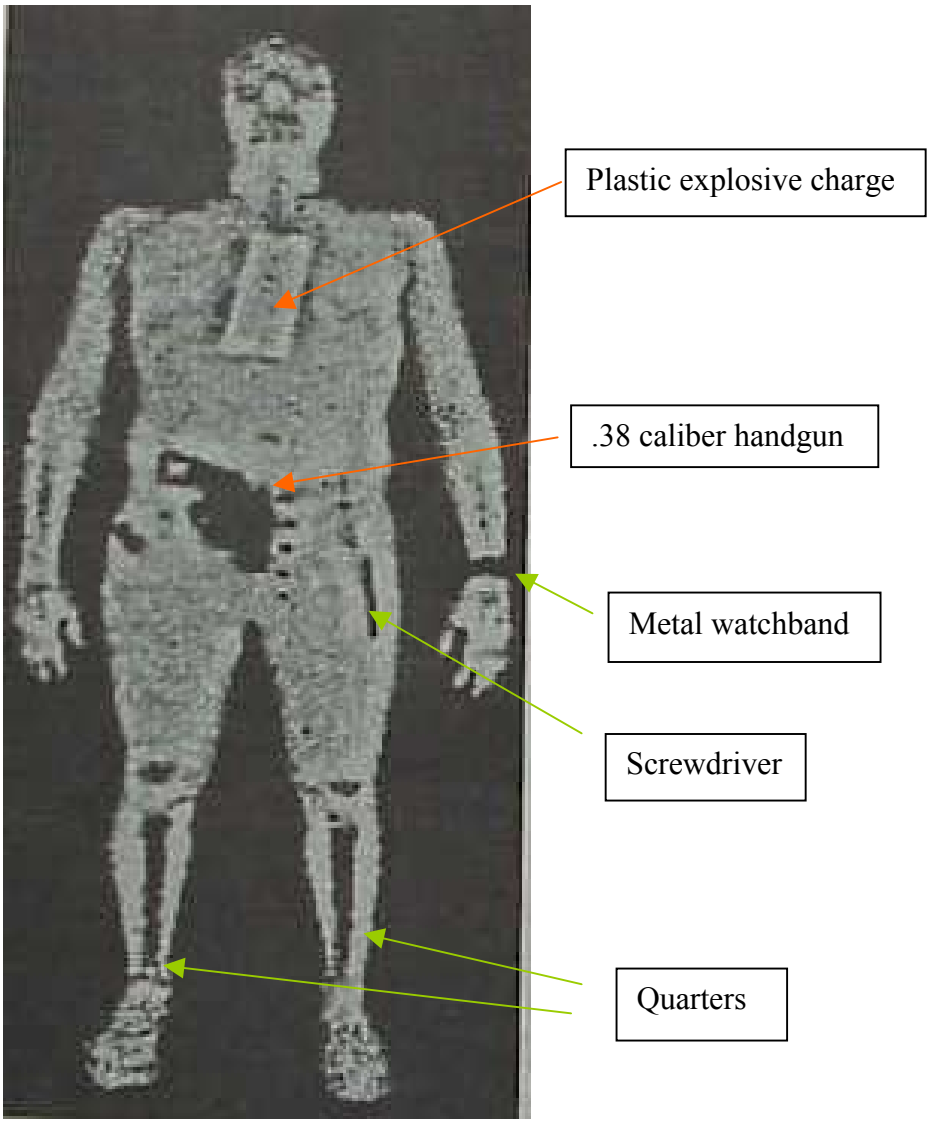

Figure 2.5-2 An image example to show the concealed objects can be identified in SECURE 1000 image system [SMI91].

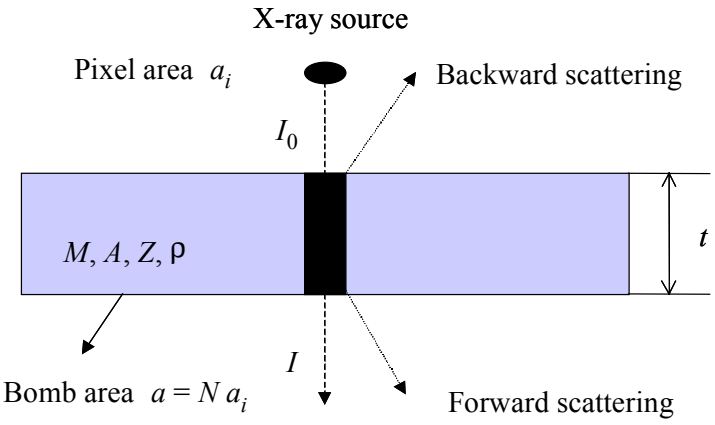

Figure 2.5-3 X-ray absorption through a rectangular block of an uniform material. The material has mass M, density ρ, thickness t, area a, atomic number Z, and atomic weight A. The incident beam flux I_0 has an area a_i so that there are $N = a/a_i$ pixels covering the block [GRO91].

$$\ln(I_{01} / I_1) = \sigma(Z, E_1) \frac{N_A}{A} \rho t \tag{2.17}$$

There are too many unknowns, such as cross section σ, density ρ, and thickness t, in Equation (2.17) to get much information from a single measurement. In particular, a thin, high Z material will have the same attenuation signal as a thick, low Z material. But two measurements obtained with two different energies can unravel some of the mystery about a single object.

At the second x-ray energy E_2, we likewise have,

$$\ln(I_{02} / I_2) = \sigma(Z, E_2) \frac{N_A}{A} \rho t \tag{2.18}$$

The division of (2.17) and (2.18) eliminates the density and thickness, and is called dual-energy which can be used to calculate the atomic number,

$$R = \frac{\ln(I_{01} / I_1)}{\ln(I_{02} / I_2)} = \sigma(Z, E_1) / \sigma(Z, E_2) \tag{2.19}$$

The dual-energy method applied to a simple object also yields the area density ρt (g/cm^2) by using either Equation (2.17) or (2.18), and in turn gives a measure of the density and the thickness by firstly using a priori knowledge between atomic number and density. But simple objects for which Equation (2.19) applies are rarely seen at airport gateways. The contents of actual luggage is infinitely varied and only occasionally neatly packed. Therefore, the dual-energy method when applied to real luggage no longer gives the atomic number of the object, but an effective atomic number Z_{eff}, and the real density is poorly known. The

term “effective atomic number” is the atomic number of that hypothetical single element which gives the same x-ray attenuation as a compound or mixture being measured.

In the real world, simple dual-energy analysis, while advantageous over single energy analysis, is easily confounded and can be hardly used for building the automated EDS. To improve the method, one must separate the objects in a complex image. Several approaches have been vigorously pursued [GRO91], such as transmission plus scattering and computer tomography. A pair of real images is shown in Figure 2.5-4. Figure 2.5-5 shows the detection result by using the method above. A potential threat, a plastic simulant obtained from FAA, is identified and displayed in red color.

2.5.3 X-ray imaging system with scatter

The two methods above only use transmission imaging techniques. Another technique used by advanced x-ray luggage inspection systems is the collection of image data from scattered x-ray energy [SCH91] [GRO91] [ANN92]. Image data may be collected from scattered x-ray energy that is reflected back towards the x-ray source or scattered x-ray energy that passed forward through the scanned object, called the back scattering and forward scattering images respectively. Systems that collect scattered x-ray image data also typically collect conventional transmission images as well.

Two characteristics of plastic explosives make them unique in their interactions with x-rays. First, they consist of elements having low atomic numbers. Second, they have a physical density about 30% - 50% higher than common plastics and five to eight times higher than typical packed clothing [ANN92]. While dual-energy methods attempt to exploit the first of these characteristics, a scatter image exploits both the low Z and high-density characteristics of plastic explosives.

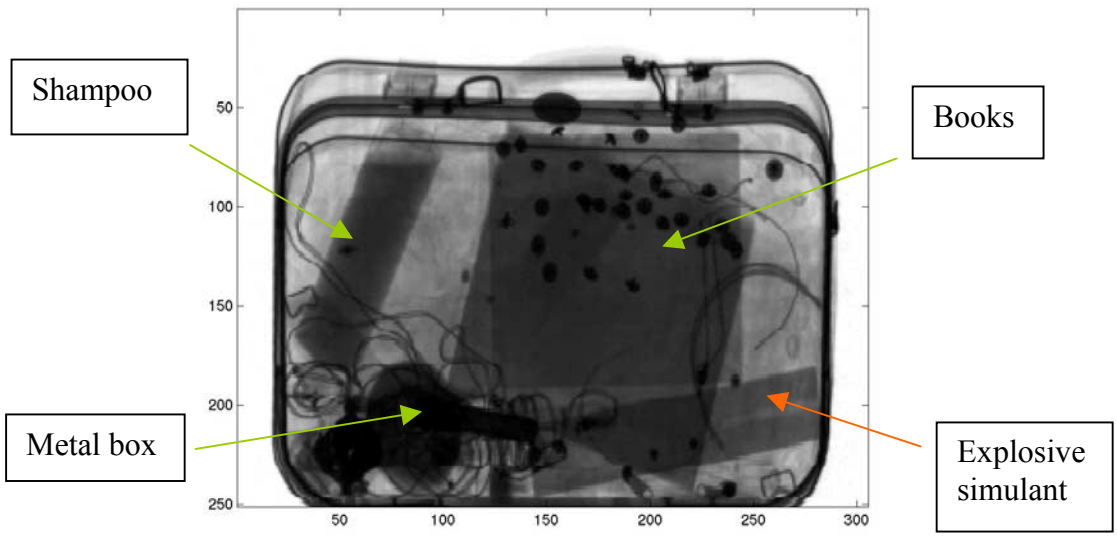

(a)

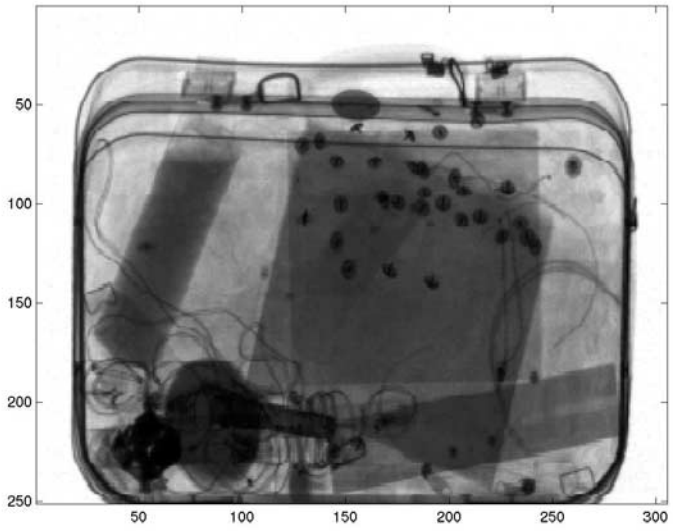

(b)

Figure 2.5-4 A pair of transmission images from a dual-energy x-ray scanning system in Virginia Tech's SDAL: (a) object scanned with input energy of 70 keV, and (b) object scanned with input energy of 140 keV.

Figure 2.5-5 A possible threat (in red color) is identified by a dual-energy x-ray machine in the SDAL of Virginia Tech.

Standard transmission imaging measures how many x-ray photons were removed from an illuminating beam at each location of the bag; it does not matter how the x-ray is removed from the pencil beam. Therefore, the atomic cross section that determines the attenuation at any location in the transmission images is the total x-ray interactive cross section – the sum of the photoelectric and the scattering cross sections.

A scatter image, however, is created in a different way and reflects the interaction cross sections differently. Each location along the pencil beam in the objects adds to the amount of scatter seen in the scatter image. The amount depends on the number of x-ray photons reaching the location, the electron density at that location, the scattering cross section, and attenuation that the scattered photons undergo while exiting the bag. Therefore, if a transmission image of objects in a bag shows that two materials have the same total attenuation, they could still have very different amounts of scatter. An example is given in Figure 2.5-6. There are two step wedges in this example, aluminum and plastic. Some of the steps shown here have a similar transmission attenuation image, but different amounts of scatter due to their different attenuation characteristics.

One technique to use scatter images was presented in [ANN92], which uses only the scatter histogram to define the threat. The reason for that is if a bag had a compact bomb hidden within it, the bomb would show up in the image as a region of intense scatter. In the histogram, it would appear as a significant increase in the number of pixels at high scatter levels.

It should be noted that three x-ray imaging systems mentioned in this section make the assumption that the transmission imaging at a particular energy is available. In Chapters 4 and 5, we will address this problem in detail.

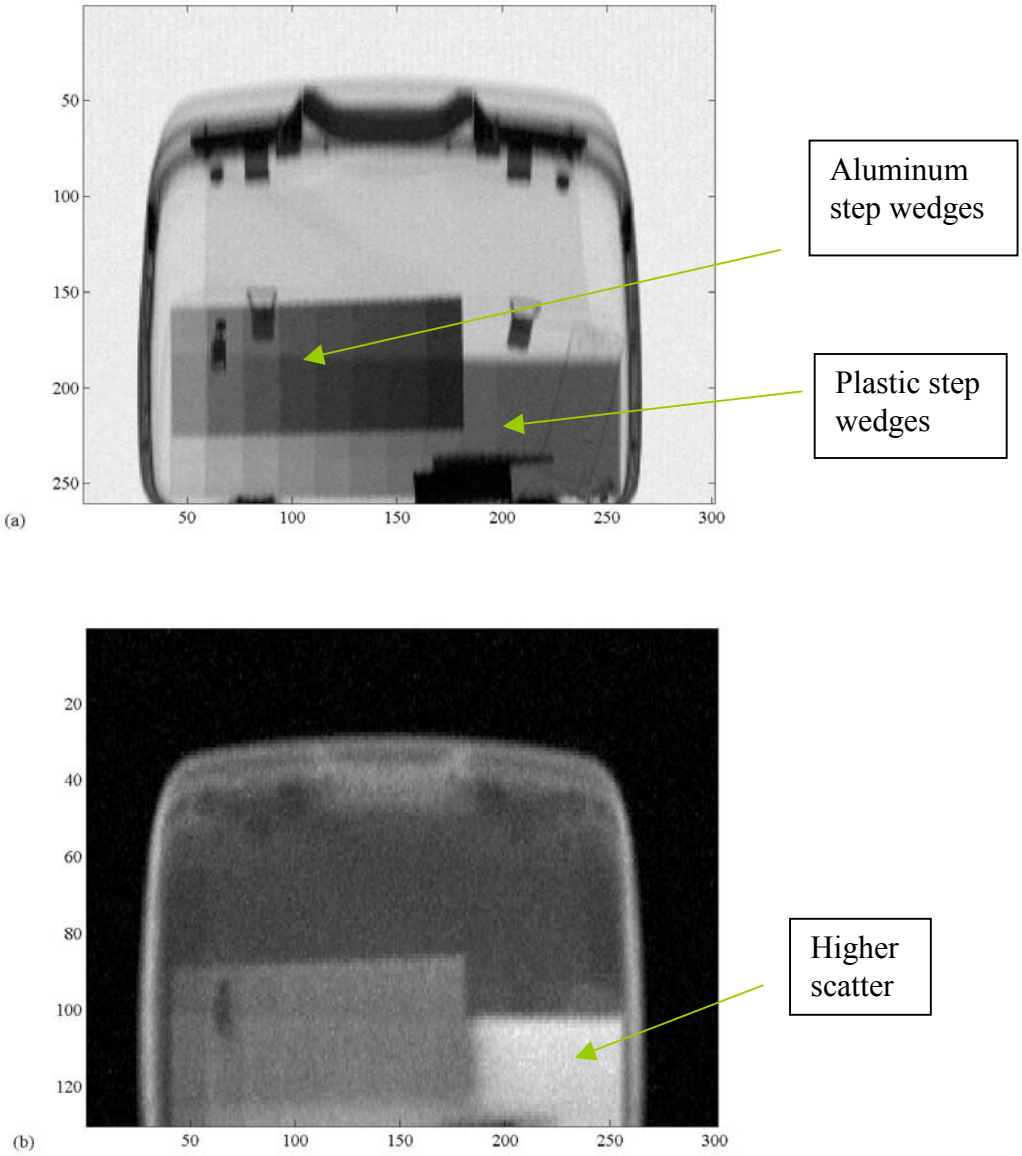

Figure 2.5-6 Transmission and scatter images scanned at the SDAL of Virginia Tech: (a) transmission image; (b) backward scatter image.

2.5.4 Computer tomography (CT) scanning system

Computed tomography, initially developed for obtaining 3-dimensional images of humans, is now being applied to the surveillance of luggage [ROD91] [ROD92] [SHR92] [SMI96]. As already stated, x-ray transmission through an object is a function of the material composition (effective atomic number), density and thickness. For each x-ray path, the total linear attenuation coefficient is the sum of the attenuation coefficients of each element in the path. CT produces cross section images of an object by reconstructing a matrix of x-ray attenuation coefficients. These images can be volume rendered to provide three-dimensional information. In the slice or volume rendered images, the reconstruction algorithm determines the linear attenuation coefficient for each volume element of the image. Since the volume element dimension is known from the geometry of the CT scanning system, the attenuation coefficient becomes a function of only two variables, effective atomic number and density. Separation of these variables is implemented with taking CT data at two x-ray energies, and essentially solving two equations for two unknowns. Thus, the volume elements can be mapped according to Z_{eff} and density, and correlation of these variables can provide both feature and material identification [DOL91].

Figure 2.5-7 gives a transmission image of a suitcase. There are coat hangers, shoes, aerosol can, simulated explosive, etc. Figures 2.5-8 through 2.5-11 show CT image reconstruction at different layers [SHR92]. By using CT techniques, a simulated explosive is clearly interpreted.

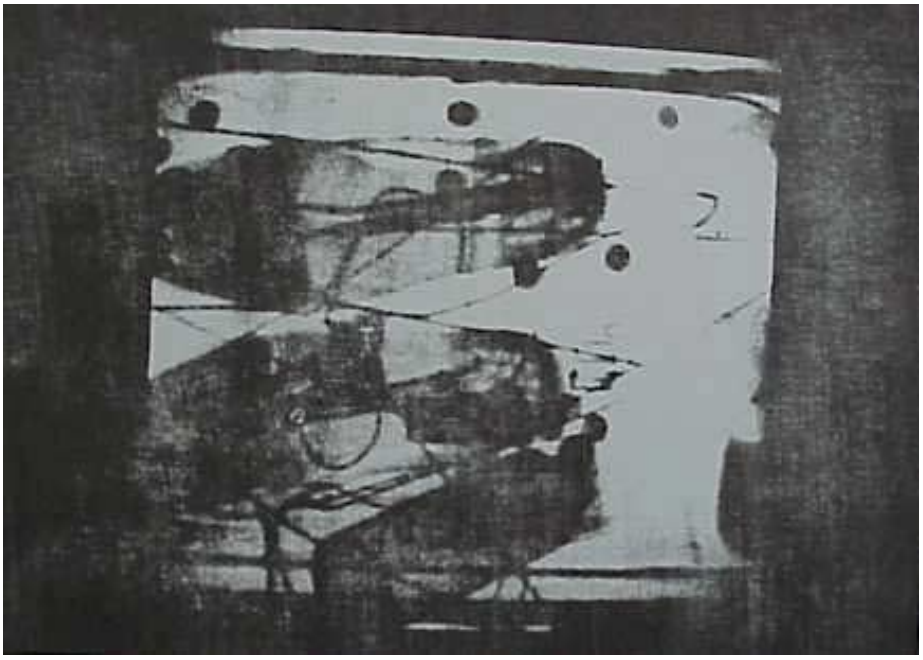

Figure 2.5-7 Transmission image of a suitcase. The dense objects such as coat hangers, shoes with shoe trees, and belt buckles, etc. are readily visible. The simulated explosive is visible, but difficult to interpret as a potential threat [SHR91].

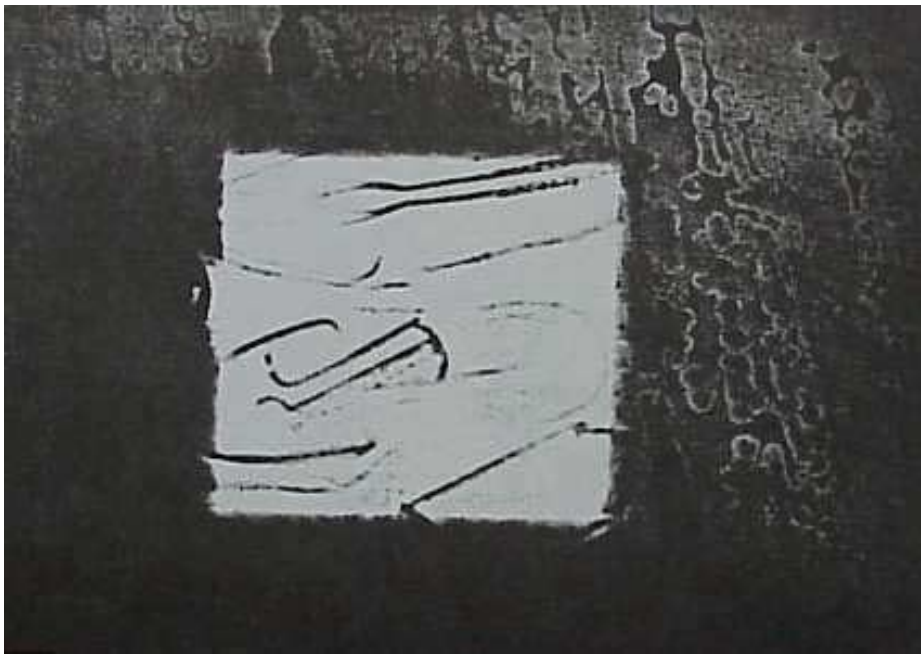

Figure 2.5-8 CT image reconstruction of a layer in the suitcase 3 inches above the bottom. The shoe trees and the top of the aerosol can are visible [SHR91].

Figure 2.5-9 CT image reconstruction of a layer in the suitcase 2.3 inches above the bottom. The heels of the shoes, coat hangers, and the aerosol can are visible [SHR91].

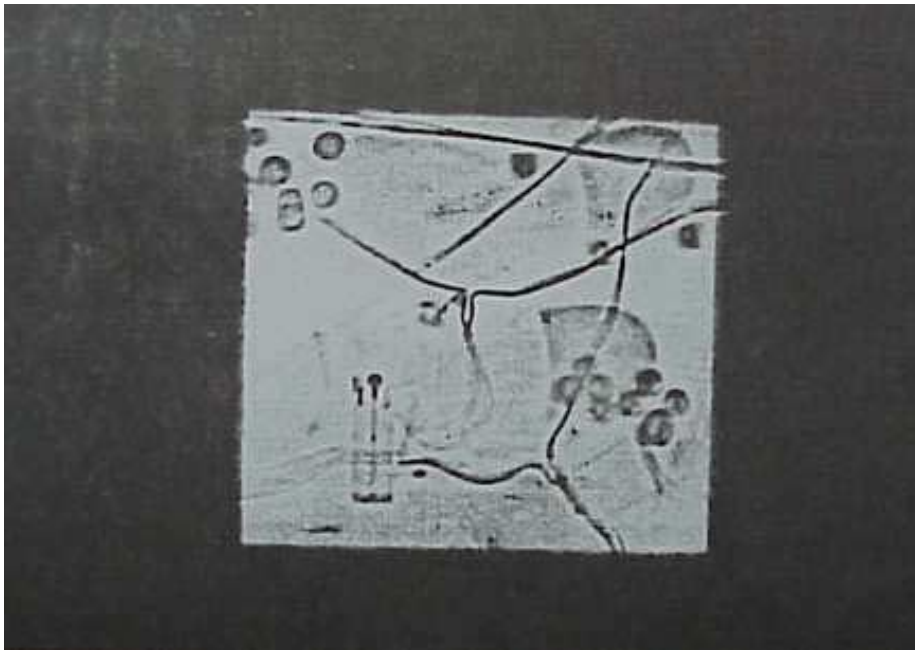

Figure 2.5-10 CT image reconstruction of a layer in the suitcase 2 inches above the bottom. The coat hangers, coins and a cigarette lighter are visible [SHR91].

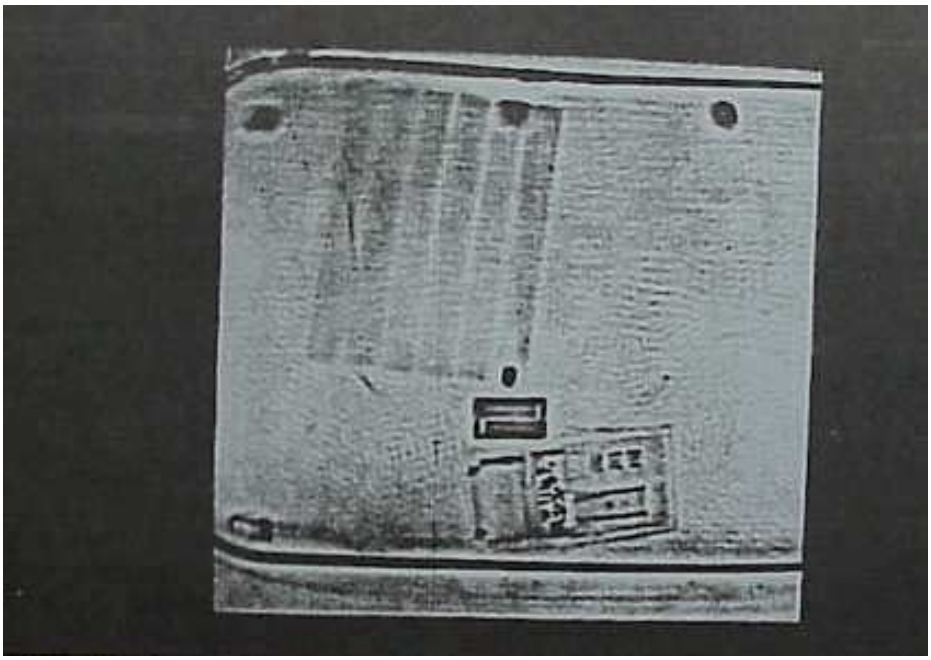

Figure 2.5-11 CT image reconstruction of a layer 0.3 inches above the bottom of the suitcase. The simulated explosive, a battery pack, a pocket calculator, and wires are clearly visible. There is a very little evidence of the overlapping structure that is apparent in the transmission image [SHR91].